

# Evidence of hydrodynamic and subdiffusive motion of tracers in a viscoelastic medium

Denis S. Grebenkov,<sup>1,\*</sup> Mahsa Vahabi,<sup>1</sup> Elena Bertseva,<sup>2</sup> László Forró,<sup>2</sup> and Sylvia Jeney<sup>2</sup>

<sup>1</sup> *Laboratoire de Physique de la Matière Condensée (UMR 7643),  
CNRS – Ecole Polytechnique, 91128 Palaiseau, France*

<sup>2</sup> *Laboratory of Physics of Complex Matter, Ecole Polytechnique Fédérale de Lausanne (EPFL),  
Station 3, CH-1015 Lausanne VD, Switzerland*

(Dated: August 9, 2021)

We propose a theoretical model which relies on the generalized Langevin equation and may account for various dynamical features of the thermal motion of organelles, vesicles or macromolecules in viscoelastic media such as polymer networks. In particular, we consider inertial and hydrodynamic effects at short times, subdiffusive scaling at intermediate times, and eventually optical trapping at long times. Simple analytical formulas for the mean square displacement and velocity auto-correlation function are derived. The developed theory is applied to the analysis of fifty-second long trajectories of micron-sized spherical tracers in actin gels that were acquired at one microsecond temporal resolution by using optical tweezers single-particle tracking. For the first time, both the subdiffusive scaling and hydrodynamic effects are observed within a single experiment and accurately described by a minimal phenomenological model.

PACS numbers: 05.40.-a, 05.10.Gg, 02.50.Ey, 47.85.Dh

Keywords: MSD, VACF, generalized Langevin equation, subdiffusion, Basset force, polymers, single-particle tracking

Single-particle tracking (SPT) techniques allow to survey individual trajectories of organelles, vesicles, macromolecules or artificial tracers in order to infer the most detailed information about their dynamics in complex or viscoelastic media, notably in living cells [1–9]. A reliable solution of this stochastic inverse problem requires the appropriate choice of a theoretical model that accurately describes all the relevant features of the dynamics (e.g., viscoelastic properties of the polymer network or the cytoskeleton, hydrodynamic interactions, and eventual optical trapping). In a simple viscous medium (e.g., water), the random trajectory  $X(t)$  of a tracer of mass  $m$  diffusing in a harmonic potential of spring constant  $k$  can be described as a solution of the Langevin equation  $m\ddot{X}(t) = F(t) + F_S(t) - kX(t)$ , in which interactions of a tracer with the surrounding bath are represented by the thermal force  $F(t)$  and the instantaneous Stokes force  $F_S(t) = -\gamma\dot{X}(t)$  with the viscous drag coefficient  $\gamma$  [10]. Two separate extensions of the Stokes force have been thoroughly studied. First, hydrodynamic interactions of a big tracer with the surrounding fluid were included by adding the Basset force which for a spherical tracer of radius  $a$  reads as [11]

$$F_B(t) = -\frac{2}{3}\pi a^3 \rho_f \ddot{X} - 6a^2 \sqrt{\pi \rho_f \eta} \int_{-\infty}^t dt' \frac{\ddot{X}(t')}{\sqrt{t-t'}}, \quad (1)$$

where  $\rho_f$  and  $\eta$  are the fluid density and viscosity (note the Stokes-Einstein relation  $\gamma = 6\pi a\eta$ ). The influence of hydrodynamic interactions which appear at short time

scales, has been thoroughly investigated, both theoretically [12–17] and experimentally [18–22]. Second, the viscoelastic properties of the medium were included by replacing the instantaneous Stokes force by a friction memory kernel  $\gamma_\alpha(t)$  [23, 24]

$$F_S(t) = - \int_{-\infty}^t dt' \gamma_\alpha(t-t') \dot{X}(t'). \quad (2)$$

In particular, a slowly decaying kernel  $\gamma_\alpha(t) = \frac{\gamma_\alpha}{\Gamma(1-\alpha)} t^{-\alpha}$  with an exponent  $0 < \alpha < 1$  leads to subdiffusive scaling of the mean square displacement (MSD) at intermediate (or long) times:  $\langle (X(t) - X(0))^2 \rangle \propto t^\alpha$ , where  $\langle \dots \rangle$  denotes the ensemble average over random realizations of the thermal force [25–31]. The subdiffusive behavior has been observed experimentally in a variety of viscoelastic media, notably in living cells [1–9]. Although the above two “mechanisms” were separately documented, neither theoretical, nor experimental investigation including both mechanisms was reported, mainly because of significantly different time scales at which both mechanisms emerge.

In this letter, we present optical tweezers experiments in which the hydrodynamic interactions and subdiffusive scaling manifest simultaneously, and a theory which accurately describes the experimental results. In particular, we derive simple analytical formulas for the MSD and the velocity auto-correlation function (VACF) that are used for fitting experimental MSD and VACF. We show that the inclusion of hydrodynamic interactions is necessary for accurate analysis of trajectories of big tracers, especially at short times (several  $\mu$ s).

The hydrodynamic interactions and subdiffusive scaling can be combined by including the Basset force (1) and

\*Electronic address: denis.grebenkov@polytechnique.edu

the Stokes force (2) into a Generalized Langevin equation (GLE). Since experimental data are available from a starting time (that we set to 0), one employs the causality principle to cut the integrals in Eqs. (1, 2) below 0. Applying the standard technique of forward and inverse Laplace transforms to this linear GLE, one gets a formal solution as [30, 31]

$$X(t) = X_0(t) + \int_0^t dt' G(t-t')F(t'), \quad (3)$$

in which the deterministic term  $X_0(t)$  (depending on the initial conditions) and the stochastic term are both determined by the linear response function  $G(t)$  which is defined through its inverse Laplace transform

$$\tilde{G}(s) = [ms^2 + \tilde{\gamma}(s)s + k]^{-1}, \quad (4)$$

where the effective friction kernel  $\tilde{\gamma}(s)$  includes both the hydrodynamic interactions and subdiffusive scaling:  $\tilde{\gamma}(s) = \frac{1}{2}m_f s + \gamma_h s^{1/2} + \gamma_\alpha s^{\alpha-1}$ , with  $\gamma_h = 6\pi a^2 \sqrt{\rho_f \eta}$  for a purely viscous medium, and  $m_f = 4\pi a^3 \rho_f / 3$  being the mass of the fluid displaced by the tracer. Both coefficients  $\gamma_\alpha$  and  $\gamma_h$  are related to the viscosity of the medium. However, finding this relation for viscoelastic media would require a microscopic model for hydrodynamic interactions that is beyond the scope of the letter.

When the thermal force  $F(t)$  is Gaussian, its distribution is fully characterized by its mean,  $\langle F(t) \rangle = 0$ , and the covariance which is related to the frictional part through the fluctuation-dissipation theorem:  $\langle F(t)F(t') \rangle = k_B T \gamma(|t-t'|)$ ,  $k_B$  being the Boltzmann's constant,  $T$  the absolute temperature [32, 33]. In that case, all the dynamical properties are fully determined by the effective kernel  $\gamma(t)$  or, equivalently, by  $G(t)$ . In particular, the exact formulas for the MSD and VACF from [30, 31] can be approximated as

$$\langle [X(t_1) - X(t_2)]^2 \rangle \simeq 2k_B T G^{(1)}(|t_1 - t_2|), \quad (5)$$

$$\langle \dot{X}(t_1)\dot{X}(t_2) \rangle \simeq k_B T g(|t_1 - t_2|), \quad (6)$$

where  $g(t)$  and  $G^{(1)}(t)$  are the derivative and the primitive of  $G(t)$ , respectively (the influence of correction terms was studied in [31]).

The practical use of the explicit relations (5, 6) requires computing inverse Laplace transform of  $\tilde{G}(s)$ . Except few particular or limiting cases, no analytical representation of  $G(t)$  is suitable for fitting experimental curves in the presence of the long memory friction kernel (i.e., with  $0 < \alpha < 1$ ). To overcome this problem, several shortcuts have been proposed such as using the Laplace transform of the experimental MSD [38] or “bypassing the foray into Laplace space” through the Fourier transform [39].

We propose a simple way to get an accurate explicit representation of the linear response function  $G(t)$  and, consequently, of the related quantities such as the MSD and VACF. For this purpose, we approximate the scaling

exponent  $\alpha$  by a rational number  $p/q$ , with integer  $p$  and  $q$ . Changing  $s$  to a new variable  $z = (s\tau)^{1/q}$  (with  $\tau$  being an appropriate time scale) allows one to represent the non-analytic function  $1/\tilde{G}(s)$  of  $s$  as a polynomial  $P(z)$  of degree  $2q$

$$\frac{\tau^2}{M\tilde{G}(s)} \equiv P(z) = z^{2q} + \frac{\gamma_h \sqrt{\tau}}{M} z^{3q/2} + \frac{\gamma_\alpha \tau^{2-\alpha}}{M} z^p + \frac{k\tau^2}{M},$$

where  $M = m + m_f/2$  is the effective mass (note that  $3q/2$  is integer by setting  $q$  to be even). For convenience, we choose the time scale  $\tau$  by setting the coefficient in front of  $z^p$  to 1:  $\tau = (M/\gamma_\alpha)^{1/(2-\alpha)}$ . The above polynomial has  $2q$  (complex-valued) roots  $z_j$ . In a general situation, all the roots are distinct (i.e.,  $z_j \neq z_k$  for  $j \neq k$ ) so that one gets  $\frac{M}{\tau^2} \tilde{G}(s) = \sum_{j=1}^{2q} \frac{A_j}{z - z_j}$ , with the coefficients  $A_j = \prod_{k \neq j}^{2q} (z_j - z_k)^{-1}$ , from which the inverse Laplace transform yields

$$G(t) = \frac{\tau}{M} \sum_{j=1}^{2q} A_j (t/\tau)^{\frac{1}{q}-1} E_{\frac{1}{q}, \frac{1}{q}}(z_j (t/\tau)^{\frac{1}{q}}), \quad (7)$$

where  $E_{\alpha, \beta}(z)$  is the Mittag-Leffler function [34, 35]. From this expression, one deduces the analytical formulas for  $G^{(1)}(t)$  and  $g(t)$  which are related to the MSD and VACF through Eqs. (5, 6):

$$G^{(1)}(t) = \frac{\tau^2}{M} \sum_{j=1}^{2q} A_j (t/\tau)^{\frac{1}{q}} E_{\frac{1}{q}, \frac{1}{q}+1}(z_j (t/\tau)^{\frac{1}{q}}), \quad (8)$$

$$g(t) = \frac{1}{M} \sum_{j=1}^{2q} A_j (t/\tau)^{\frac{1}{q}-2} E_{\frac{1}{q}, \frac{1}{q}-1}(z_j (t/\tau)^{\frac{1}{q}}). \quad (9)$$

The integral representation of Mittag-Leffler functions [34] can be used for a rapid and accurate numerical computation of  $G^{(1)}(t)$  and  $g(t)$ .

The above model includes the known explicit solutions:

(i) normal diffusion of a massive tracer ( $\alpha = 1$  and  $\gamma_h = 0$ ) corresponds to  $p = q = 1$  for which  $E_{1,1}(z) = e^z$  and thus  $G(t) = (A_1 e^{z_1 \gamma_1 t/M} + A_2 e^{z_2 \gamma_1 t/M})/\gamma_1$ , with  $z_{1,2} = -\frac{1}{2}(1 \pm \sqrt{1 - 4kM/\gamma_1^2})$ . When  $M \rightarrow 0$ , it reduces to  $G(t) = e^{-kt/\gamma_1}/\gamma_1$ .

(ii) normal diffusion of a massive tracer with hydrodynamic interactions ( $\alpha = 1$  and  $\gamma_h \neq 0$ ) is obtained for  $p = q = 2$ , for which the functions  $E_{\frac{1}{2}, \frac{n}{2}}(z)$  can be expressed through  $E_{\frac{1}{2}, 1}(z) = e^{z^2} \text{erfc}(-z)$  that yields the classical formulas for the MSD and VACF [14, 18, 22] (here  $\text{erfc}(z)$  is the complementary error function).

(iii) when there is no optical trapping ( $k = 0$ ), some roots  $z_j$  are zero so that one gets another representation  $\frac{M}{\tau^2} \tilde{G}(s) = \frac{1}{z^p} \sum_j \frac{\bar{A}_j}{z - z_j}$ , in which  $\bar{A}_j = \prod_{k \neq j}^{2q} (z_j - z_k)^{-1}$  and the sum and product are taken over all nonzero roots  $z_j$

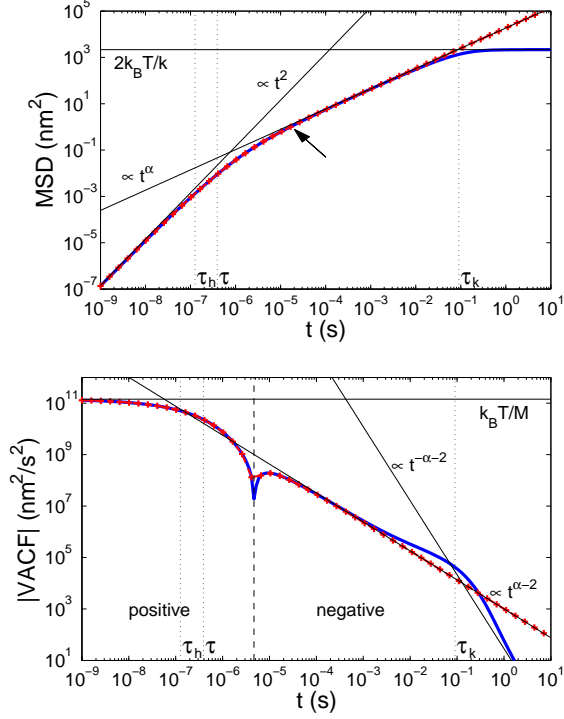


FIG. 1: (Color online) Theoretical time-averaged MSD and VACF of a spherical tracer in a viscoelastic medium. Curves from Eqs. (8, 9) are shown by thick solid blue line ( $\alpha = 7/8$ ,  $k = 3.77 \cdot 10^{-6}$  N/m,  $\gamma_\alpha = 4.6 \cdot 10^{-7}$  kg/s<sup>9/8</sup>,  $\gamma_h = 8.0 \cdot 10^{-11}$  kg/s<sup>1/2</sup>,  $M = 2.84 \cdot 10^{-14}$  kg); curves from Eqs. (11) without optical trapping ( $k = 0$ ) are shown by red crosses, and the asymptotic behaviors at different time scales are shown by thin black lines. Vertical dotted lines locate three characteristic time scales  $\tau_h$ ,  $\tau$  and  $\tau_k$ , while the vertical dashed line separates the regions with positive and negative values of the VACF. The arrow indicates the region where the inertial and hydrodynamic effects lead to deviations from the subdiffusive scaling.

of the polynomial  $P(z)$ . The Laplace inversion of this relation yields

$$G(t) = \frac{\tau}{M} \sum_j \bar{A}_j(t/\tau)^{\frac{1+p}{q}-1} E_{\frac{1}{q}, \frac{1+p}{q}}(z_j(t/\tau)^{\frac{1}{q}}), \quad (10)$$

from which

$$\begin{aligned} G^{(1)}(t) &= \frac{\tau^2}{M} \sum_j \bar{A}_j(t/\tau)^{\frac{1+p}{q}} E_{\frac{1}{q}, \frac{1+p}{q}+1}(z_j(t/\tau)^{\frac{1}{q}}), \\ g(t) &= \frac{1}{M} \sum_j \bar{A}_j(t/\tau)^{\frac{1+p}{q}-2} E_{\frac{1}{q}, \frac{1+p}{q}-1}(z_j(t/\tau)^{\frac{1}{q}}). \end{aligned} \quad (11)$$

The classical formulas for  $\alpha = 1$  can be retrieved by setting again  $p = q = 2$  [12, 13]. In turn, for subdiffusion with  $\gamma_h = 0$ , the above formula reduces to  $G(t) = \frac{t}{M} E_{2-\alpha, 2}(-(t/\tau)^{2-\alpha})$  [29–31].

Using the properties of Mittag-Leffler functions and relations for the roots  $z_j$  of the polynomial  $P(z)$ , one

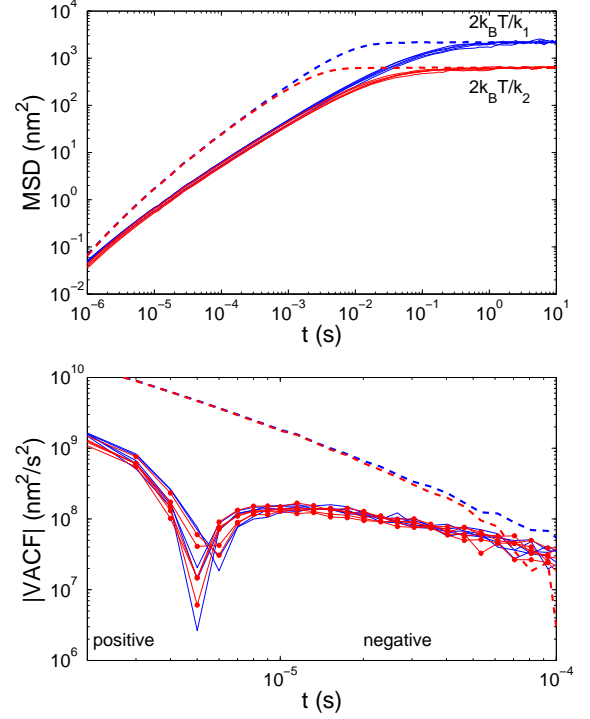


FIG. 2: (Color online) Experimental time-averaged MSD and VACF of a spherical tracer in water (dashed curves) and in an actin gel for the weak (group of blue solid curves) and strong (group of red solid curves) optical traps, with trap constants  $k_1$  and  $k_2$ , respectively. Five curves in each group show the results for five acquisitions. Red full circles are added for the VACF plot in order to better distinguish two groups.

can derive the asymptotic behavior of  $G(t)$  (and thus the MSD and VACF) at different time scales (Fig. 1):

$$\begin{aligned} G(t) &\simeq \frac{t}{M} - \frac{4\gamma_h t^{\frac{3}{2}}}{3\sqrt{\pi}M^2} + \frac{\gamma_h^2 t^2}{2M^3} - \frac{8\gamma_h^3 t^{\frac{5}{2}}}{15\sqrt{\pi}M^4} + \dots (t \ll \tau_h), \\ G(t) &\simeq \frac{t^{\alpha-1}}{\gamma_\alpha \Gamma(\alpha)} - \frac{\gamma_h t^{2\alpha-\frac{5}{2}}}{\gamma_\alpha^2 \Gamma(2\alpha-\frac{3}{2})} + \dots (\tau \ll t \ll \tau_k), \\ G(t) &\simeq \frac{\gamma_\alpha t^{-\alpha-1}}{|\Gamma(-\alpha)|k^2} + \frac{\gamma_\alpha^2 t^{-2\alpha-1}}{\Gamma(-2\alpha)k^3} - \frac{3\gamma_h t^{-\frac{5}{2}}}{4\sqrt{\pi}k^2} + \dots (t \gg \tau_k), \end{aligned}$$

where  $\tau_k = (\gamma_\alpha/k)^{1/\alpha}$  is the trapping time and  $\tau_h = (M/\gamma_h)^2$  is the characteristic time for hydrodynamic interactions. For normal diffusion ( $\alpha = 1$ ), one retrieves the classical behavior:  $g(t) \simeq \frac{\gamma_h}{2\sqrt{\pi}\gamma_1^2} t^{-3/2}$  [12] for  $k = 0$  and  $g(t) \simeq \frac{15\gamma_h}{8\sqrt{\pi}k^2} t^{-7/2}$  for  $k > 0$  [14].

In order to verify the influence of hydrodynamic interactions on subdiffusion of big tracers, the trajectories of a spherical bead immersed in an actin gel were recorded. The experimental set-up has been described in [36, 37]. The actin filaments were reconstituted from the pre-formed actin filaments (Cytoskeleton, Inc. AKF99-A) by dissolving in 2 ml of Milli-Q water. This gives the concentration of 0.5 mg/ml in the following buffer:

6 mM Tris-HCl pH 8.0, 0.24 mM  $\text{CaCl}_2$ , 0.24 mM ATP, 2.4 mM  $\text{MgCl}_2$  and 6% (w/v) sucrose. The  $3\text{ }\mu\text{m}$  diameter melamine resin beads (Microparticles GmbH, S1712) were added to water beforehand. The actin filaments with beads have been placed between a microscope slide and a coverslip separated by  $200\text{ }\mu\text{m}$  spacers. The obtained sample chamber was divided into two parts: one for actin, and the other for pure water. Both solutions contained the same kind of tracers.

The measurements in water served as a reference for calibration of the trap. The time-averaged MSD was computed from the position fluctuation signal recorded in volts and fitted by  $2k_B T \beta^2 G^{(1)}(t)$  with  $G^{(1)}(t)$  given by Eq. (8) with  $p = q = 2$  (i.e.,  $\alpha = 1$ ),  $\rho_f = 1000\text{ kg/m}^3$  (water density),  $\rho = 1510\text{ kg/m}^3$  (melamine resin density),  $\eta = 0.959 \cdot 10^{-3}\text{ kg/m/s}$  (dynamic viscosity of water at  $T = 295\text{ K}$ ),  $a = 1.5\text{ }\mu\text{m}$  (bead radius). The only fitting parameters were the spring constant  $k$  and the volt-to-meter conversion factor  $\beta$ . For two laser powers, we obtained  $k_1 = 3.77 \cdot 10^{-6}\text{ N/m}$  (weak trap) and  $k_2 = 1.28 \cdot 10^{-5}\text{ N/m}$  (strong trap), respectively. Subsequently, all MSDs recorded in the actin gel were renormalized to get the same long-time plateau value  $2k_B T/k$  of the time-averaged MSD as for beads in water.

After calibration, the time-averaged MSD and VACF are calculated separately for each bead as

$$\mathcal{M}(t) \equiv \frac{1}{N-n} \sum_{k=1}^{N-n} [X((k+n)\delta) - X(k\delta)]^2, \quad (12)$$

$$\mathcal{V}(t) \equiv \frac{\delta^{-2}}{N-n-1} \sum_{k=1}^{N-n-1} [X((k+1)\delta) - X(k\delta)] \times [X((k+n+1)\delta) - X((k+n)\delta)], \quad (13)$$

where  $X(t)$  is the coordinate of the bead at time  $t$ ,  $N$  is the number of points of the acquired trajectory,  $t = \delta n$  is the lag time, and  $\delta$  is the time step of data acquisition. In the set-up,  $\delta = 1\text{ }\mu\text{s}$  and  $N = 5 \cdot 10^7$  (fifty-second long trajectories).

Figure 2 shows the time-averaged MSD and VACF of a spherical tracer in an actin gel. The first group of blue solid curves corresponds to five trajectories in the weak optical trap, while the second group of red curves corresponds to five trajectories in the strong optical trap. The curves from each group are close to each other. Deviations between curves within one group can be attributed to heterogeneities in the actin gel. Note also that the curves from both groups are close to each other at small times at which the optical trap is negligible. For comparison, the MSD and VACF for the same bead in water are shown by black dashed lines.

The characteristic feature of big tracers at short times is a clear deviation from the subdiffusive scaling with the exponent  $\alpha$  at intermediate times (in the range  $10^{-5} - 10^{-2}\text{ s}$ ). The VACF is particularly sensitive to this deviation which is caused by the inertial and hydrodynamic effects. In fact, the MSD and VACF of a massless tracer are respectively  $\frac{2k_B T}{k}(1 - E_{\alpha,1}(-kt^\alpha/\gamma_\alpha))$  and

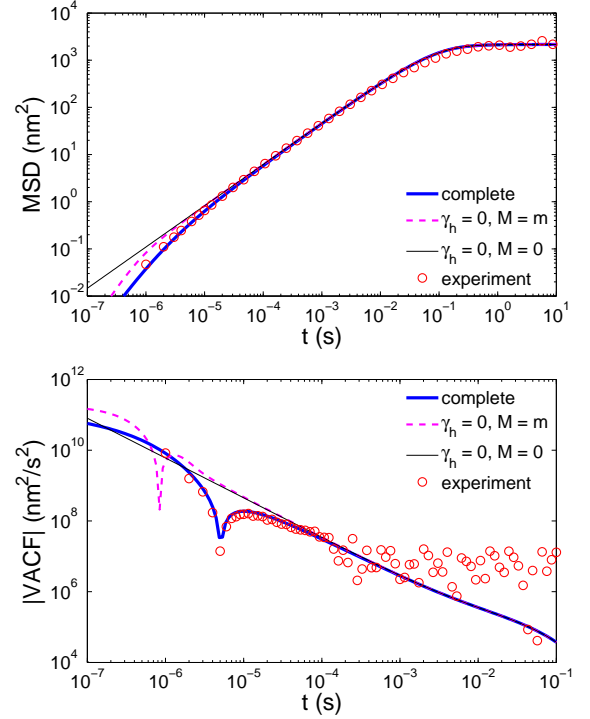


FIG. 3: (Color online) Experimental time-averaged MSD and VACF of a spherical tracer in an actin gel (circles) compared with three theoretical models: the complete model (anomalous diffusion with hydrodynamic interactions; shown by solid blue curve), and its two simplified versions, in which the hydrodynamic interactions and then the inertial effects are neglected. The model parameters are:  $k = k_1$ ,  $\alpha = 7/8$ ,  $\gamma_\alpha = 4.38 \cdot 10^{-7}\text{ kg/s}^{9/8}$ ,  $\gamma_h = 8.0 \cdot 10^{-11}\text{ kg/s}^{1/2}$ ,  $M = 2.84 \cdot 10^{-14}\text{ kg}$ .

$\frac{k_B T}{\gamma_\alpha} t^{\alpha-2} E_{\alpha,\alpha-1}(-kt^\alpha/\gamma_\alpha)$  that for short times behave as  $\frac{\gamma_\alpha}{2D_\alpha} t^\alpha$  and  $\frac{-D_\alpha}{\Gamma(\alpha-1)} t^{\alpha-2}$ , where  $D_\alpha = k_B T/\gamma_\alpha$  is the generalized diffusion coefficient [30, 31]. In particular, this VACF is always negative showing anti-persistence in random displacements of a massless tracer. In turn, the inertial and hydrodynamic effects ensure that the VACF becomes positive at short time. The change of sign of the VACF at  $t = 5 - 6\text{ }\mu\text{s}$  is clearly seen on Fig. 2.

Searching for a minimal phenomenological model to describe the motion of big spherical tracers in actin gels, one may question whether the inclusion of the hydrodynamic interactions is relevant or not. In other words, would it be sufficient to include only the inertial term  $ms^2$  but neglect the term  $\gamma_h s^{3/2}$ ? Figure 3 illustrates the importance of the hydrodynamic interactions. We compare the experimental MSD and VACF (circles) for one trajectory with the theoretical curves obtained from the complete model (i.e., when both the inertial and hydrodynamic effects are included), and two simplified models, in which one first neglects the hydrodynamic interactions (setting  $\gamma_h = 0$  and  $M = m$ ) and then ignores inertial effects (setting  $\gamma_h = 0$  and  $M = 0$ ). One can see that the theoretical

MSD and VACF from Eqs. (8, 9) (referred to as complete model) correctly reproduce the experimental ones over 7 orders of magnitude in time (the range being narrower for the VACF, for which the experimental values become hidden by intrinsic fluctuations at  $t > 10^{-4}$  s). Deviations between complete and simplified models for the MSD are relatively small though visible for the lag time above  $1 \mu\text{s}$  (the range accessible in our experiment). In turn, the deviations are much more explicit for the VACF. We conclude that the hydrodynamic interactions become significant for big tracers (of radius above one micron) and at time scales below tens of microseconds. The explicit formulas (8, 9) allow one to reveal the respective roles of various forces and mechanisms and to choose the appropriate model for a reliable analysis of SPT trajectories of endogeneous or artificial tracers in complex viscoelastic media such as polymer networks and living cells.

In conclusion, we presented a minimal phenomenological model which accounts for inertial and hydrodynamic effects at short times, subdiffusive scaling at intermedi-

ate times, and optical trapping at long times. All these features have to be included in order to get accurate fits to the experimental time-averaged MSD and VACF of big tracers in actin gels when the lag time  $t$  ranges from one microsecond (the acquisition time step in our setup) to tens of seconds (the measurement duration). We emphasize on the phenomenological character of the model in which intricate interactions of a tracer with actin filaments network are effectively characterized by the scaling exponent  $\alpha$  and the coefficients  $\gamma_\alpha$  and  $\gamma_h$ . Microscopic models and/or molecular dynamics simulations are needed to relate these phenomenological parameters to mechanical properties of the actin network. The advantage of the phenomenological model is that the derived analytical formulas are explicit and easy to compute through integral representations of the Mittag-Leffler functions, while the model can be further extended to incorporate other mechanisms (e.g., adding the term  $s\gamma_1$  to  $1/\tilde{G}(s)$  to treat separately the contributions from the solvent,  $\gamma_1$ , and from the polymer networks,  $\gamma_\alpha$ ).

- 
- [1] I. M. Tolić-Nørrelykke, E.-L. Munteanu, G. Thon, L. Oddershede, and K. Berg-Sørensen, Phys. Rev. Lett. **93**, 078102 (2004).
  - [2] I. Golding, E. Cox, Phys. Rev. Lett. **96**, 098102 (2006).
  - [3] D. Arcizet, B. Meier, E. Sackmann, J. O. Rädler, and D. Heinrich, Phys. Rev. Lett. **101**, 248103 (2008).
  - [4] C. Wilhelm, Phys. Rev. Lett. **101**, 028101 (2008).
  - [5] D. Wirtz, Ann. Rev. Biophys. **38**, 301-326 (2009).
  - [6] J. Szymanski and M. Weiss, Phys. Rev. Lett. **103**, 038102 (2009).
  - [7] R. Metzler, V. Tejedor, J.-H. Jeon, Y. He, W. H. Deng, S. Burov, E. Barkai, Acta Phys. Pol. B **40**, 1315 (2009).
  - [8] J.-H. Jeon, V. Tejedor, S. Burov, E. Barkai, C. Selhuber-Unkel, K. Berg-Sørensen, L. Oddershede, and R. Metzler, Phys. Rev. Lett. **106**, 048103 (2011).
  - [9] E. Bertseva, D. S. Grebenkov, P. Schmidhauser, S. Gribkova, S. Jeney, and L. Forró, Eur. Phys. J. E **35**, 63 (2012).
  - [10] W. T. Coffey, Y. P. Kalmykov, and J. T. Waldron, *The Langevin equation: with applications to stochastic problems in physics, chemistry and electrical engineering*, 2nd Ed. (World Scientific Publishing, Singapore, 2004).
  - [11] A. B. Basset, *A treatise on hydrodynamics, with numerous examples* (Cambridge, Deighton, Bell and Co., 1888).
  - [12] A. Widom, Phys. Rev. A **3**, 1394-1396 (1971).
  - [13] E. J. Hinch, J. Fluid Mech. **72**, 499-511 (1975).
  - [14] H. J. H. Clercx and P. P. J. M. Schram, Phys. Rev. A **46**, 1942 (1992).
  - [15] F. Mainardi and P. Pironi, Extr. Math. **11**, 140 (1996).
  - [16] T. Indei, J. D. Schieber, and A. Córdoba, Phys. Rev. E **85**, 041504 (2012).
  - [17] T. Indei, J. D. Schieber, A. Córdoba, and E. Pilyugina, Phys. Rev. E **85**, 021504 (2012).
  - [18] B. Lukić, S. Jeney, Z. Sviben, A. J. Kulik, E.-L. Florin, and L. Forró, Phys. Rev. E **76**, 011112 (2007).
  - [19] T. Franosch, M. Grimm, M. Belushkin, F. M. Mor, G. Foffi, L. Forró, and S. Jeney, Nature **478**, 85 (2011).
  - [20] R. Huang, I. Chavez, K. M. Taute, B. Lukić, S. Jeney, M. G. Raizen, and E.-L. Florin, Nat. Phys. **7**, 576 (2011).
  - [21] M. Grimm, S. Jeney and T. Franosch, Soft Matter **7**, 2076 (2011).
  - [22] M. Grimm, T. Franosch and S. Jeney, Phys. Rev. E **86**, 021912 (2012).
  - [23] H. Mori, Prog. Theor. Phys. **33**, 423 (1965).
  - [24] W. Hess and R. Klein, Adv. Phys. **32**, 173-283 (1983).
  - [25] J. M. Porrà, K.-G. Wang, and J. Masoliver, Phys. Rev. E **53**, 5872-5881 (1996).
  - [26] K. G. Wang and M. Tokuyama, Phys. A **265**, 341 (1999).
  - [27] E. Lutz, Phys. Rev. E **64**, 051106 (2001).
  - [28] N. Pottier, Physica A **317**, 371-382 (2003).
  - [29] A. D. Vinales and M. A. Desposito, Phys. Rev. E **73**, 016111 (2006).
  - [30] M. A. Desposito and A. D. Vinales, Phys. Rev. E **80**, 021111 (2009).
  - [31] D. S. Grebenkov, Phys. Rev. E **83**, 061117 (2011).
  - [32] R. Kubo, M. Toda, and N. Hashitsume, *Statistical physics II. Nonequilibrium statistical mechanics* (Springer, 1985).
  - [33] R. Zwanzig, *Nonequilibrium Statistical Mechanics* (Oxford University Press, New York, 2001).
  - [34] R. Gorenflo, J. Loutchko, Y. Luchko, Fract. Calc. Appl. Anal. **5**, 491-518 (2002).
  - [35] H. J. Haubold, A. M. Mathai, and R. K. Saxena, J. Appl. Math. **2011**, 298628 (2011).
  - [36] E. Bertseva et al., Nanotechnology **20**, 285709 (2009).
  - [37] S. Jeney, F. Mor, R. Koszali, L. Forró and V. T. Moy, Nanotechnology **21**, 255102 (2010).
  - [38] T. Mason and D. Weitz, Phys. Rev. Lett. **74**, 1250 (1995).
  - [39] R. M. L. Evans, M. Tassieri, D. Auhl, and T. A. Waigh, Phys. Rev. E **80**, 012501 (2009).